

Bayesian Low-Rank LeArning (Bella): A Practical Approach to Bayesian Deep Learning

Bao Gia Doan^{1*}, Afshar Shamsi^{2*}, Xiao-Yu Guo¹, Arash Mohammadi²,
Hamid Alinejad-Rokny³, Dino Sejdinovic¹, Damien Teney⁴, Damith Ranasinghe¹,
Ehsan Abbasnejad¹

¹The University of Adelaide, Australia

²Concordia University, Canada

³UNSW Sydney, Australia

⁴Idiap Research Institute, Switzerland

Abstract

Bayesian learning has demonstrated merits in robustness and resilience to unseen and out-of-distribution inputs, yet its adoption in large-scale tasks remains limited. In particular, deep ensemble methods (Seligmann et al. 2024; Lakshminarayanan, Pritzel, and Blundell 2017) have proven to be highly effective, but they suffer from a high computational cost. This paper introduces an alternative framework that mitigates the computational burden of ensemble Bayesian deep learning. The approach is inspired by the recent success of low-rank adapters and is named Bayesian Low-Rank LeArning (Bella). We show that (1) Bella achieves a dramatic reduction in the number of trainable parameters required to approximate a Bayesian posterior; and (2) it not only maintains, but in some instances surpasses the performance—in accuracy and out-of-distribution generalisation—of conventional Bayesian and non-Bayesian methods. An extensive empirical evaluation on large-scale tasks (ImageNet, CAMELYON17, DomainNet, VQA) with CLIP and LLaVA demonstrates the effectiveness and versatility of Bella in building scalable and Bayesian deep models for real-world applications.

1 Introduction

Bayesian deep learning (Neal 2012) provides mechanisms for building predictive models that are more robust to adversarial attacks, resilient to unseen and out-of-distribution inputs, and a principled approach for estimating model uncertainty (Liu et al. 2019; Ye and Zhu 2018; Wilson et al. 2022; Izmailov et al. 2020; Chen and Ghattas 2020). In particular, quantifying uncertainty enables more reliable decision-making and facilitates identifying potential model vulnerabilities in uncertain regions of the input space. Therefore, Bayesian deep learning (BDL) has a high potential in helping build more reliable and trustworthy AI systems for various real-world applications (e.g., autonomous driving, medical image analysis, etc.). Unfortunately, BDL methods suffer from a high computational complexity.

Bayesian models contrast with traditional point estimates, i.e. a single set of parameters representing a single mapping from inputs to outputs. A Bayesian model, instead, learns a *distribution* of model parameters that captures a

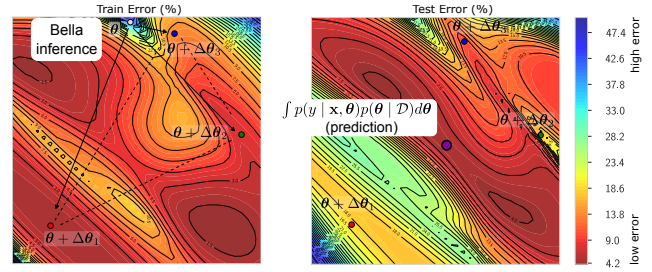


Figure 1: Training (left) and test (right) error landscapes on the CAMELYON17 dataset (%). The left figure shows a learned 3-particle approximation of the modes of the posterior of a pre-trained model θ . The test landscape is slightly different from the training one, highlighting the challenge of generalization. While a point estimate does not generalize well (a single parameter particle such as $\theta + \Delta\theta_1$) Bella shows a clear benefit. The Bayesian prediction (Equation (1)) effectively averages over multiple parameter settings and leads to lower test error.

distribution over possible predictions. Let us consider a neural network $f(\mathbf{x}, \theta)$ with input \mathbf{x} parameterized by θ and its corresponding prior distribution $p(\theta)$. The likelihood $p(\mathcal{D}|\theta)$ is determined by f (Bishop 2006) and Bayesian inference uses Bayes’ theorem to derive a *posterior* distribution $p(\theta|\mathcal{D}) = p(\mathcal{D}|\theta)p(\theta)/p(\mathcal{D})$ and then compute the predictive distribution:

$$p(y|\mathbf{x}, \mathcal{D}) = \int p(y | \mathbf{x}, \theta)p(\theta | \mathcal{D})d\theta. \quad (1)$$

Despite evidence for the benefits of Bayesian learning, its adoption is hindered by several challenges, most importantly the intractability of the posterior distribution $p(\theta|\mathcal{D})$ in most practical tasks. The exact solution is impractical to compute even for networks of moderate size, hence the necessity of using approximations.

This paper expands upon recent research demonstrating the effectiveness of ensemble methods and Stein Variational Gradient Descent (SVGD) (Liu and Wang 2016) approaches in BDL (Seligmann et al. 2024; Lakshminarayanan, Pritzel, and Blundell 2017; Abbasnejad et al. 2020a; Doan et al. 2022; Izmailov et al. 2020; Chen and Ghattas 2020). These methods aim to provide a practical method for ensemble Bayesian

*These authors contributed equally.

deep learning for large-scale tasks. With the goal of achieving a practical and efficient approach, we consider spawning parameter particles (models) by adding linear interpolation to a pre-trained model’s parameters to an ensemble. To further enhance the efficiency of these interpolations, we take inspiration from low-rank adaptation (LoRAs)(Hu et al. 2022) and propose to use low-rank parameters in the interpolation process. We therefore name the approach Bayesian Low-Rank Learning (Bella).

We validated Bella by comparing it to the full-parameter alternative in terms of (1) accuracy, (2) out-of-distribution generalization, (3) adversarial robustness, and (4) alignment of uncertainty estimation with human confidence. In summary, our findings indicate that our approach achieves comparable performance to full SVGD or ensemble methods at a fraction of the computational cost, with the exception of adversarial robustness. For example, Figure 1 illustrates the application of our proposed approach of Bayesian inference in an application with distribution shifts (CAMELYON17 (Koh et al. 2021) benchmark). The particles (*i.e.*, parameter samples from the posterior) obtained using Bella prove effective in improving generalization, improving the common single particle fine-tuning and comparable with full ensemble-based baselines at a fraction of the cost. Our key contributions are:

- We propose a new Bayesian learning framework, Bella, for SVGD approximation of a posterior—exploiting the availability of pre-trained models, we spawn particles or models by linear interpolation of a constrained set of model parameters for a SVGD approximation of a posterior.
- Our approach more efficiently captures the complexity and multi-modality of the solution space compared to current SVGD but at a fraction of the cost—we observe on-par performance with full SVGD in uncertainty estimation, performance improvement, and robustness but only use less than 0.3% of parameters.
- We demonstrate Bella to perform on par or better than baselines—ensembles or current SVGD implementations. Bella consistently outperforms the non-BNN counterparts on 8 datasets; image classification (ImageNet, CIFAR 10/100), Out-of-distribution (DomainNet, Camleyon17, CIFAR-10-C), and VQA as well as *adversarial robustness*. Notably, it sets a new state-of-the-art on CAMELYON17 (see Table 7 and the Camelyon leaderboard (2024)).
- Bella employed with the multi-modal model LLaVa (Liu et al. 2023b) leads to improved performance and uncertainty estimation highly correlated with human confidence.

2 Related Work

Parameter-Efficient Fine Tuning. In contrast to fine-tuning all parameters, recent research proposed inserting *adapters* in between existing neural layers to reduce the number of trainable parameters and, subsequently, the compute (GPU consumption) (Houlsby et al. 2019; Rebuffi, Bilen, and Vedaldi 2017; Lin, Madotto, and Fung 2020). Hu et al. (Hu et al. 2022) use a bottleneck structure to impose a low-rank constraint on the weight updates, named LoRA. The key functional difference is that LoRA can be merged with the main weights

during inference, thus avoiding the introduction of any latency whilst significantly reducing the number of parameters. **Fine-Tuning Approaches and Bayesian Deep Learning.** Previous research investigating the application of fine-tuning approaches for BDLs have predominantly focused on large language models (LLMs), e.g. (Fan et al. 2020; Zhang et al. 2021; Yang et al. 2024). Notably, marking a departure from the conventional methods relying primarily on tuning the network’s parameters, these studies chose to define priors and approximate posterior over low rank *attention weights*. Concurrently, Yang et al. (Yang et al. 2024) introduced the concept of Laplace LoRA to incorporate Bayesian concepts to enhance the calibration of fine-tuned LLMs. However, Laplace’s method (Daxberger et al. 2021) relies on a Gaussian approximation of the posterior distribution. Whilst this can be effective for unimodal and symmetric distributions, the approach does not fully encapsulate the intricacies of more complex posteriors, particularly in neural networks where the posterior has multimodality and asymmetry (Izmailov et al. 2021). Deep ensembles (Lakshminarayanan, Pritzel, and Blundell 2017) typically perform better in practice compared with variational and Laplace methods, due to their ability to capture multiple modes. When employing fine-tuning, a direct application of ensembling for LoRAs was considered in (Wang, Aitchison, and Rudolph 2024). Some interpretations of deep ensembles suggest that they approximate gradient flows in function spaces and that building desirable properties into an ensemble (such as repulsive behavior), is possible (Wild et al. 2023). SVGD (Liu and Wang 2016), can be viewed in a similar vein. However, while these more sophisticated, repulsive, ensembling approaches are highly impractical in the pre-training phase, we argue that their expressivity can be brought to bear precisely in tandem with low-rank fine-tuning, which is the viewpoint we adopt in this contribution.

Building upon these foundations, our research represents a pioneering effort to apply the principles of repulsive ensemble-based low-rank fine-tuning to computer vision. In particular, we bridge pre-training and fine-tuning phases with recent conjectures on mode connectivity (Ainsworth, Hayase, and Srinivasa 2023). Our methodology not only capitalizes on the efficiency of fine-tuning techniques, e.g. (Ding et al. 2023, 2022; Dettmers et al. 2023) but also innovatively addresses the scalability challenges inherent to BDLs. Overall, our work sets a new precedent in applying Bayesian approaches to computer vision tasks by offering a scalable and efficient framework for enhancing model performance.

3 Background on

Stein Variational Gradient Descent (SVGD)

Bayesian inference techniques have been integral to the development of neural networks, with a rich history underscored by previous works (Neal et al. 2011; Neal 2012; MacKay 1991; Welling and Teh 2011; Blei, Kucukelbir, and McAuliffe 2017). Variational Inference (VI) (Blundell et al. 2015; Blei, Kucukelbir, and McAuliffe 2017) and Markov Chain Monte Carlo (MCMC) (Neal et al. 2011; Welling and Teh 2011) are two primary approximate Bayesian inference frameworks.

The former substitutes the true posterior with a tractable alternative while the latter involves sampling. However, accurately computing the posterior with either MCMC or VI becomes computationally infeasible when dealing with large-scale networks containing millions of parameters. Although approximations can be obtained more efficiently with VI (Blundell et al. 2015), VI is also demonstrably too restrictive to resemble the *multi-modality* of the true posterior and suffers from mode collapse (Izmailov et al. 2021).

Stein Variational Gradient Descent (SVGD) (Liu and Wang 2016), among other ensemble-based approaches, is an alternative approximate Bayesian technique that combines the strengths of MCMC and VI by transporting a set of parameter *particles* to fit the true posterior distribution, while encouraging diversity among the particles, by incorporating a repulsive term in the parameter updates. This diversity prevents the mode collapse and enables learning multiple models to represent various patterns in the data. Using n samples from the posterior (*i.e.* parameter particles), SVGD modifies the gradient descent as:

$$\begin{aligned} \boldsymbol{\theta}_i &= \boldsymbol{\theta}_i - \epsilon_i \hat{\phi}^*(\boldsymbol{\theta}_i) \quad \text{with} \\ \hat{\phi}^*(\boldsymbol{\theta}) &= \sum_{j=1}^n [k(\boldsymbol{\theta}_j, \boldsymbol{\theta}) \nabla_{\boldsymbol{\theta}_j} \log p(\boldsymbol{\theta}_j | \mathcal{D}) - \frac{\gamma}{n} \nabla_{\boldsymbol{\theta}_j} k(\boldsymbol{\theta}_j, \boldsymbol{\theta})]. \end{aligned}$$

Here, $\boldsymbol{\theta}_i$ is the i th particle, $k(\cdot, \cdot)$ is a kernel function that measures the similarity between particles and γ is a hyper-parameter. Notably, the kernel function encourages the particles to be dissimilar in order to capture more diverse samples from the posterior and γ controls the trade-off between the diversity of the samples versus the minimization of the loss.

4 Bayesian Low-Rank Learning (Bella)

The problem with the current SVGD and other ensemble-based methods in large deep neural networks is its huge computational cost. This renders it infeasible to train efficiently and to scale to a sufficient number of parameter particles for accurately approximating the posterior distribution, which currently remains coarse. In this work, we propose to capitalize on the low-rank representations of fine-tuning in order to construct a practical and scalable variant of SVGD. We note that while our approach may not fully capture the diversity of the multi-modal posterior, a recent conjecture (Ainsworth, Hayase, and Srinivasa 2023) suggests that these modes might result from parameter permutations in neural networks, leading to models that are functionally equivalent. Building on this idea, Bella could serve as a practical alternative with sufficient theoretical justification for ensemble methods.

Consider any dense layer, for which there is a fixed pre-trained weight matrix $\boldsymbol{\theta}_0 \in \mathbb{R}^{d_1 \times d_2}$ with d_1, d_2 the corresponding numbers of hidden units. We consider n low-rank perturbations of $\boldsymbol{\theta}_0$ as

$$\boldsymbol{\theta}_i = \boldsymbol{\theta}_0 + \Delta\boldsymbol{\theta}_i = \boldsymbol{\theta}_0 + \mathbf{B}_i \mathbf{A}_i, \quad i = 1, \dots, n. \quad (2)$$

where $\mathbf{B}_i \in \mathbb{R}^{d_1 \times r}$, $\mathbf{A}_i \in \mathbb{R}^{r \times d_2}$ are the low-dimensional update parameters, and $r \ll d_1, d_2$ is the rank of the update. Now Bella proceeds as the joint SVGD on $(\mathbf{A}_i, \mathbf{B}_i)$, with updates

$$\mathbf{A}_i = \mathbf{A}_i - \epsilon_i \sum_{j=1}^n \hat{\phi}_j^*(\mathbf{A}_i), \quad \mathbf{B}_i = \mathbf{B}_i - \epsilon_i \sum_{j=1}^n \hat{\phi}_j^*(\mathbf{B}_i)$$

$$\begin{aligned} \text{with } \hat{\phi}_j^*(\mathbf{B}_i) &= k_{i,j} \nabla_{\mathbf{B}_i} p(y | \mathbf{x}, \boldsymbol{\theta}_0 + \mathbf{B}_i \mathbf{A}_i) - \frac{\gamma}{n} \nabla_{\mathbf{B}_i} k_{i,j}, \\ \hat{\phi}_j^*(\mathbf{A}_i) &= k_{i,j} \nabla_{\mathbf{A}_i} p(y | \mathbf{x}, \boldsymbol{\theta}_0 + \mathbf{B}_i \mathbf{A}_i) - \frac{\gamma}{n} \nabla_{\mathbf{A}_i} k_{i,j}, \end{aligned}$$

where we denote $k_{i,j} = k(\mathbf{B}_j \mathbf{A}_j, \mathbf{B}_i \mathbf{A}_i)$. Here, we have placed a zero-mean Gaussian prior on $(\mathbf{A}_i, \mathbf{B}_i)$, but other choices are possible. Note that the kernel function on $(\mathbf{A}_i, \mathbf{B}_i)$ is given by $k(\boldsymbol{\theta}_0 + \mathbf{B}_j \mathbf{A}_j, \boldsymbol{\theta}_0 + \mathbf{B}_i \mathbf{A}_i)$, which ensures that the similarity is computed on the original parameter space, and in the commonly used case of shift-invariant kernels, this simplifies to $k(\mathbf{B}_j \mathbf{A}_j, \mathbf{B}_i \mathbf{A}_i)$. Further simplifications are obtained for specific kernel functions – in particular, in the case of Gaussian RBF, while the naive implementation would require the cost of $O(rd_1 d_2)$ for a single kernel evaluation, we can bring it down to $O(r^2(d_1 + d_2))$ using standard trace manipulation, as described in the Appendix G. This procedure can be repeated across all dense layers.

Bella introduces a significant improvement in the efficiency of model training and execution. By utilizing the same pre-trained weights $\boldsymbol{\theta}_0$ across all parameter particles but allowing for individual low-rank adaptations $\Delta\boldsymbol{\theta}_i$, we achieve a balance between parameter sharing and the diversity necessary for effective learning. Bella significantly reduces the parameter space from the full matrix’s $d_1 d_2$ to just $r(d_1 + d_2)$, thereby enhancing both efficiency and scalability. This setup not only reduces the computational burden during training but also streamlines the process at inference time. The heavy lifting is done once by loading the large base model $\boldsymbol{\theta}_0$, and the lightweight low-rank adapters $\Delta\boldsymbol{\theta}_i$ can be dynamically applied with minimal overhead in order to approximate the posterior predictive distribution as $p(y^* | \mathbf{x}^*, \mathcal{D}) \approx \frac{1}{n} \sum_{i=1}^n p(y^* | \mathbf{x}, \boldsymbol{\theta}_0 + \Delta\boldsymbol{\theta}_i)$. This approach is particularly advantageous in large-scale models, where the weight matrices $\boldsymbol{\theta}_0$ are of substantial dimensions.

5 Experiments and Results

In this section, we provide an in-depth overview of our experimental setup, detailing the methodology, equipment, and procedures employed in the implementation of Bella. We aim to compare Bella with established ensemble-based methods and SVGD, both of which have demonstrated effectiveness in BDLs (Seligmann et al. 2024; Lakshminarayanan, Pritzel, and Blundell 2017).

5.1 Experimental Setup

Datasets. In this research, we have employed a variety of datasets, each selected for their relevance and contribution, they include CIFAR-10, CIFAR-100 (Krizhevsky, Hinton et al. 2009), CIFAR-10-C (Hendrycks and Dietterich 2019), STL-10 (Coates, Ng, and Lee 2011), CAMELYON17 (Bandi et al. 2018), ImageNet (Russakovsky et al. 2015), and DomainNet (Peng et al. 2019). We also consider VQA v2 dataset utilized for Visual Question Answering (VQA). Additional details are in Appendix I and Appendix H.

Neural Architecture. In our experiments, we employed the CLIP ViT-B/32 model (Ilharco et al. 2021), a pre-trained variant utilizing contrastive supervision from image-text pairs, as initially introduced in the seminal CLIP research (Radford et al. 2021). We conducted end-to-end fine-tuning of

Datasets	Bella Models		Baseline Models (Base)			
	Ensemble (n=5)	SVG D (n=5)	Ensemble (n=5)	SVG D (n=5)	Single	VBL
CIFAR10	97.32 ± 0.37%	97.57 ± 0.38%	97.26 ± 0.28%	<u>97.56</u> ± 0.31%	96.86 ± 0.43%	94.04 ± 0.37%
CIFAR100	86.02 ± 0.48%	87.63 ± 0.46%	86.65 ± 0.24%	<u>87.03</u> ± 0.29%	85.14 ± 1.3%	85.01 ± 1.21%
CAMELYON17	93.11 ± 1.36%	<u>93.61</u> ± 1.28%	93.29 ± 0.94%	93.98 ± 1.23%	90.25 ± 2.31%	91.58 ± 1.38%
DomainNet	80.34 ± 2.36%	81.41 ± 3.06%	<u>82.96</u> ± 2.11%	83.66 ± 1.76%	69.75 ± 4.86%	80.60 ± 2.37%
ImageNet	77.29	78.24	<u>78.93</u>	79.36	76.87	-

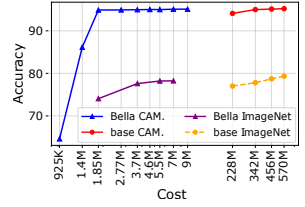


Figure 2: **Left:** Comparing performance of Bella models with their baseline (*Base*) counterparts on *vision benchmarks*. The results confirm Bella models are well-performing and on par with their baseline Ensemble, SVG D, and VBL whilst consuming only a fraction of cost (see Table 1 grey columns for corresponding costs). The best-performing results are in **bold**, the second-best in underline, and the least favorable are in *italic* for emphasis. **Right:** Bella achieves similar Accuracy with full SVG D (Base) only with a fraction of cost.

the image encoder, adjusting all model parameters, a strategy typically yielding higher accuracy than training only the final linear layer. For both our ensemble-based methods, we consider conventional ensemble and SVG D. We use the average logits (unnormalized outputs) to produce the output (Gontijo-Lopes, Dauphin, and Cubuk 2021). For VQA task, we employ the SoTA LLaVA-1.5-7B (Liu et al. 2023b) to showcase the effectiveness of Bella on large-scale network architecture. Details of the hyper-parameters are discussed in Appendix I.

5.2 Cost Efficiency

The accuracy comparison of our Bella models with their respective base models, as well as with Vision Bayesian Lora (VBL)—a derived Laplace’s approximation from (Yang et al. 2024) for vision tasks—is delineated in the left table in Figure 2. The respective costs comparison on training (in terms of trainable parameters) is shown in Table 1—notably, the grey columns are the ones used for generating the results in the left table in Figure 2.

Impressively, across a spectrum of benchmark computer vision datasets such as CIFAR-10, CIFAR-100, Camelyon17, and ImageNet, the Bella models demonstrate superior performance. This is achieved with only a fraction of cost (trainable parameters) as shown in Table 1, underscoring the models’ proficiency in parameter efficiency without compromising on accuracy. Further, the Bella models surpass the performance of *Single* models, while employing a comparable level of computational resources—see the Memory Consumption of models used, in Table 1 reporting approximately 4.5 GB for Bella compared to 5.05 GB for Single. The results across the benchmarks attest to the efficacy of our methodology.

Notably, in Section 5.1 with Bella SVG D, with 1.6% of the trainable parameters in comparison to the Single baseline, leads to approximately 2% and 10% increase in performance on the OOD tasks of DomainNet and CAMELYON17, respectively; whilst achieving comparable performance with the current SVG D implementation (SVG D baseline model).

Along with Section 5.1, Table 1 demonstrates the primary benefit of our approach—the *significant reduction in memory and storage needs*. For example, Table 1, we obtain approximately a 5× reduction in model size—that is from 2,222 MB for a 5 particle SVG D baseline model to just 440 MB for a

Bella SVG D model with 5 particles. This efficiency not only reduces the demands on GPUs but also minimizes potential I/O bottlenecks.

Moreover, the reduced GPU demand, as shown in Table 1, facilitates larger mini-batch sizes during training to speedup the training process. More crucially, it enables the enhancement of the Bayesian posterior’s parameter particles to over 100, a feat previously unattainable with current SVG D implementations. Significantly, constructing a 100 parameter Bayesian approximation consumes only 5.19 GB memory compared to current SVG D implementations for Bayesian models (SVG D base) needing over 6 GB for *even a merely 3 particle approximation*.

Interestingly, our on-par results of Bella models with current SVG D and ensemble approximations of the posterior provide empirical evidence that with constrained model parameters, it is still possible to reach the diverse modes of the posterior. Further, *the results support recent conjectures on mode connectivity* (Gueta et al. 2023).

5.3 Out-Of-Distribution (OOD) Datasets

Assessing the robustness of machine learning systems to unseen conditions is crucial, particularly regarding their ability to generalize to out-of-distribution (OOD) data. We evaluate robustness to OOD by utilizing multiple OOD benchmarks and estimating accuracy under various noise levels (distribution shifts) to further assess the performance of different baselines in these challenging scenarios.

First, we use the DomainNet dataset, which is one of the most diverse domain adaptation datasets and spans a wide range of visual styles, from real images to abstract art. This variety provides a challenging test bed for algorithms aiming to bridge different visual domains. Our study involves training the CLIP network on the ‘Real’ subset of DomainNet and evaluating its generalization across various domains. Additionally, we use CIFAR-10-C, a corrupted version of CIFAR-10, to further assess the generalization and robustness of models trained on CIFAR-10 datasets. The results for both datasets are presented in ??.

Furthermore, the STL-10 dataset, which has significant label overlap with CIFAR-10, serves as a relevant OOD test case for CIFAR-10 models (see Appendix B).

Results from ?? and Appendix B show that Bella models, demonstrating significantly better efficiency, achieve competi-

Models	Bseline Models (SVGD)				Bella Models (SVGD)				Single
	$n=3$	$n=5$	$n=20$	$n=40$	$n=3$	$n=5$	$n=20$	$n=100$	$n=1$
Trainable Parameters	340M	567M	1.76B	3.51B	1.10M	1.84M	7.37M	36.86M	113M
Memory Consumption (RAM in GB)	6.71	8.35	26.08	48.45	4.48	4.50	4.63	5.19	5.05
Storage Consumption (MB)	1321	2222	8868	17735	436	439	460	572	433

Table 1: Computational cost to train different models based on CLIP architecture for different datasets. Notably, with SVGD Baseline Models, we can only train up to $n=40$ particles on a A6000 48 GB GPU, while we can increase to more than 100 parameter particles with our Bella method with negligible increase of GPU consumption. The grey columns correspond to costs (parameters) of models in Figure 2.

Models	DomainNet						Avg.	CIFAR-10-C			Avg.
	Real	Clip-Art	Infograph	Paint	Sketch	Gaussian Blur		Pixelate	Spatter		
Single base	74.61	55.29	31.81	53.87	43.84	51.89	90.58	77.94	92.14	78.53	
VBL	82.97	59.94	26.56	52.81	46.96	53.85	89.34	76.43	89.21	70.76	
Ensemble Bella	82.70	61.22	28.15	55.32	51.58	55.60	93.30	85.86	94.83	82.24	
Ensemble base	85.07	65.40	36.07	57.90	54.22	59.73	91.92	86.49	93.45	84.61	
SVGD Bella	84.47	63.67	32.22	56.83	54.86	58.41	94.05	88.70	94.85	83.77	
SVGD base	85.42	65.53	36.58	58.18	55.47	60.24	93.02	86.75	95.19	86.84	

Table 2: The out-of-distribution generalization performance of Bella, measured by accuracy (for number of particles $n=5$). Each column represents a specific shift, either real (DomainNet) or artificial (CIFAR-10-C). Further results can be found in Appendix D.

tive performance compared to more resource-intensive implementations with Ensemble and SVGD baselines across both DomainNet and CIFAR-10-C benchmarks. All Bayesian approximations, including our scalable and efficient method, outperform the single model baseline.

5.4 Comparing Uncertainty Estimations

Bayesian models capable of providing a theoretical basis for measuring *model uncertainty*. Also known as epistemic uncertainty, refers to uncertainty stemming from limitations in our knowledge or understanding of the underlying data generating process or the model itself. One of the ways to quantify model uncertainty is through mutual information estimates, following (Gal et al. 2016).

Mutual Information (MI). This is the mutual information between the output prediction and the posterior over model parameters θ , and can be used as a measure of epistemic (model) uncertainty. It can be expressed as: $\text{MI}(\theta, y | \mathcal{D}, \mathbf{x}) = H[p(y | \mathcal{D}, \mathbf{x})] - \mathbb{E}_{p(\theta | \mathcal{D})} H[p(y | \theta, \mathbf{x})]$ If the parameters at input are well defined (e.g., data seen during training), then we would gain little information from the obtaining label, or the MI measured will be low.

We employ MI to measure uncertainty to investigate whether the Bella approximations of the posterior leads to uncertainty estimates commensurate with those obtained from SVGD baselines. This provides empirical evidence of a functional equivalence of the Bella approximations of the posterior to that obtained from the current computationally intensive implementation of SVGD.

Datasets. We utilize the CIFAR-10-C task, featuring corrupted images, to examine the uncertainty of model predictions trained on the standard CIFAR-10 dataset. Additionally, we assess the uncertainty measures on the CAMELYON17 dataset, which is characterized by inherent dataset shifts within itself.

Results. Figure 3 demonstrates the effectiveness of our approach to estimate uncertainty. Our Bella perform similarly to the SVGD base model, with a slightly better uncertainty

on misclassified images of CAMELYON17 and corrupted CIFAR-10-C datasets (under brightness corruption with the maximum intensity), see details and other corruption types in Appendix C.

5.5 Robustness against Adversarial Examples

In this section, we examine the resilience of our proposed Bella against adversarial attacks, specifically employing the L_∞ Fast Gradient Sign Method (FGSM) across various attack budgets as detailed in Figure 4. This analysis aims to benchmark the robustness of our method in comparison to traditional models under adversarial conditions. We employ the robustness benchmark (Papernot et al. 2018) to deploy the attack on CIFAR-10 test set and report results in Figure 4.

The findings presented in Figure 4 reveal that conventional models such as SVGD and Ensemble exhibit just slightly greater resistance to adversarial attacks. We attribute this enhanced robustness to the broader diversity in model parameters, which stems from their capacity to adjust the entire network’s parameters, unlike the Bella models.

Significantly, despite operating within the same computational constraints as a singular network model, our Bella demonstrates enhanced efficacy in mitigating adversarial attacks, thereby bolstering its robustness.

5.6 Ablation Studies

This section undertakes a series of ablation studies to examine the effects of various components within Bella. Our analysis includes an exploration of the training costs associated with different ranks and their consequent influence on model performance. Given that Bella incorporates multiple parameter particles, we also delve into how varying the number of these particles affects Bella’s efficacy. Additionally, we explore the application of low-rank adapters across different layers and assess their impact. Further details on other studies are in Appendix E. We show in Table 7 that we achieve state-of-the-art performance on CAMELYON17.

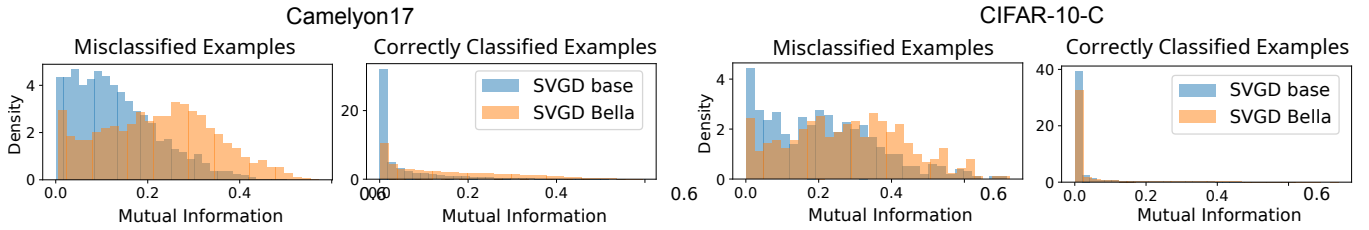


Figure 3: Evaluation of uncertainty estimations using Mutual Information on CAMELYON17 and CIFAR-10-C datasets. \uparrow MI for Misclassified Examples is better—denoted by the distribution shifting \rightarrow . In contrast, \downarrow MI for Correctly Classified Examples is better—denoted by the distribution shifting \leftarrow . Notably, Single base models are not able to capture *epistemic* uncertainty (Gal et al. 2016).

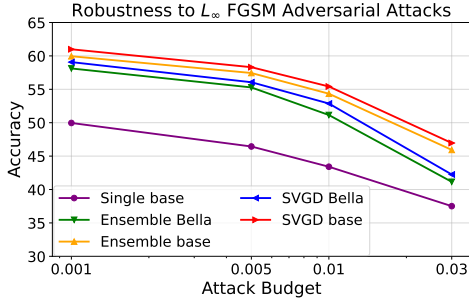


Figure 4: Comparison of model robustness to L_∞ FGSM adversarial attacks across varied attack budgets. The evaluation is on the CIFAR-10 dataset. Bella achieves comparable performance to current, baseline SVGD and Ensemble (number of particles is equal to 5) implementations whilst demonstrating significantly better robustness (higher accuracy) than a Single baseline model.

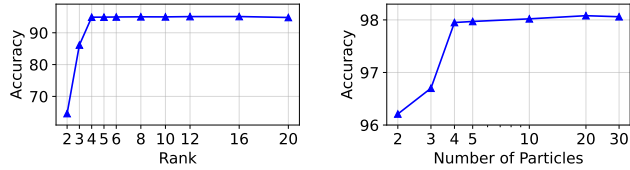


Figure 5: The impact of ranks on CAMELYON17 performance (left), as well as the impact of the number of parameter particles on CIFAR-10 (right) on Bella performance.

Ablations on rank r . As outlined in Section 4, we substitute the network’s extensive full matrix with low-rank matrices defined by the ‘rank’ parameter (r). This section aims to assess how this parameter influences Bella’s performance.

To thoroughly assess the influence of rank, we conduct our analysis on the challenging large-scale CAMELYON17 dataset. The results, depicted in Figure 5 (left), elucidate the relationship between rank size and performance. While utilizing a smaller rank considerably reduces the parameter space, it also restricts Bella’s learning capacity, hindering its ability to achieve optimal performance. In contrast, increasing the rank to 4 significantly enhances Bella’s efficiency. However, performance tends to plateau at a rank of 16, indicating a saturation point.

Ablations on the number of particles n . In this section, we delve into the influence of the quantity of parameter particles on the performance of Bella. The findings, depicted

in the right in Figure 5, reveal an improvement in Bella’s performance with an increase in the number of particles.

This outcome is both intuitive and insightful, as a larger ensemble of parameter particles enhances the approximation of the Bayesian posterior more effectively.

Ablations on the number of trainable parameters. We will compare the number of trainable parameters between Bella and full SVGD in model performance. Critically, higher number of trainable parameters means higher cost to train. To show generalization, we also employ another large-scale challenging dataset Imagenet in this experiment.

The plot in Figure 2 (right) for the CAMELYON17 dataset begins with Bella at $r = 2$ (comprising 5 particles) and concludes with full SVGD (SVGd base) using the same number of particles. As r increases, the accuracy of Bellas improves, eventually plateauing at approximately 95.08%, which is comparable to the accuracy of full SVGD (95.21%). This highlights the efficiency and advantages of our proposed Bella. Remarkably, Bella achieves performance on par with full SVGD models despite utilizing a significantly smaller pool of trainable parameters—approximately 0.3% for $r = 4$ —compared to the more parameter-intensive alternatives.

Datasets	Metrics	Bella Models		Baseline Models (Base)				
		Ens.	SVGd	Single	VI	SGLD	Ens.	SVGd
CIFAR10	ECE \downarrow	1.4	1	8.1	0.99	<u>0.94</u>	2.5	0.55
	MCE \downarrow	65	26	35	33	24	<u>23</u>	21
	Brier \downarrow	0.40	0.32	0.49	0.43	0.36	0.49	<u>0.33</u>
	AUROC \uparrow	99.98	99.99	99.78	99.93	99.94	99.99	99.99
CIFAR100	ECE \downarrow	5.2	4.9	6.5	4.2	<u>3.8</u>	5.1	3.3
	MCE \downarrow	19	15	86	47	41	48	46
	Brier \downarrow	0.23	<u>0.19</u>	0.23	0.2	<u>0.19</u>	<u>0.19</u>	0.18
	AUROC \uparrow	99.88	99.88	99.71	99.87	99.83	99.88	99.88
CAMELYON17	ECE \downarrow	5.5	5.3	6.4	<u>5</u>	5.2	5.3	4.9
	MCE \downarrow	31	<u>29</u>	34	36	31	30	21
	Brier \downarrow	5.2	<u>5.1</u>	5.5	5.4	5.4	<u>5.1</u>	4.5
	AUROC \uparrow	98.4	<u>98.7</u>	98.12	98.6	98.6	98.5	98.81
DomainNet	ECE \downarrow	5.9	5.8	7.9	5.1	<u>4.6</u>	5.2	4.9
	MCE \downarrow	40	<u>37</u>	61	40	41	<u>37</u>	34
	Brier \downarrow	5.3	5.2	6.3	<u>5</u>	4.4	<u>5</u>	4.7
	AUROC \uparrow	98.31	98.46	98.1	98.99	99.21	98.88	<u>99.01</u>

Table 3: Calibration comparison of Bella models (SVGd and Ensemble) with baseline methods across multiple datasets. The evaluation considers calibration metrics (ECE, MCE) and discriminative capability (Brier Score, AUROC). Lower values for ECE, MCE, and Brier Score, along with higher values for AUROC, indicate better performance.

Calibration Study. Table 3 presents a comparison of the Bella models (SVG D and ensemble) against baseline models, including Variational Inference (VI) (Kim and Hospedales 2023) and Stochastic-Gradient Langevin Dynamic (SGLD) (Welling and Teh 2011), using several key metrics: Expected Calibration Error (ECE), Maximum Calibration Error (MCE), Brier score, and Area Under the Receiver Operating Characteristic curve (AUROC). Lower ECE and MCE values indicate that the model’s probability estimates are more reliable. A lower Brier score reflects better accuracy in the model’s probability predictions, while a higher AUROC demonstrates superior discrimination between classes. Across the datasets, the Bella models demonstrate performance comparable to the baseline models. This suggests that the Bella models, while utilizing far fewer parameters for training, offer a strong alternative to traditional baseline approaches while maintaining competitive calibration and Discriminative capability.

5.7 Visual Question Answering

In this section, we extend the application of our Bella to another challenging vision task, Visual Question Answering (VQA), as detailed in (Antol et al. 2015). We leverage the state-of-the-art, pre-trained, large multi-modal model LLaVA (Liu et al. 2023b,a) for this purpose. Utilizing LLaVA transforms VQA into a process where an image and a natural-language question are inputs, and the model generates a free-form, open-ended text answer. Answering questions in VQA requires various intelligent capabilities, including not only image recognition but also complex reasoning. For this task, we employ VQA v2 (Antol et al. 2015) dataset containing 204,721 images, more than 1 Billion (1B) questions and 10B ground-truth answers in total. There are three main types of answers: Yes/No, a Number, and Other.

Model. In our experiments, we employed our proposed Bella on top of LLaVA-1.5-7B (Liu et al. 2023b,a). Further details about the dataset, model and metrics are deferred to Appendix H.

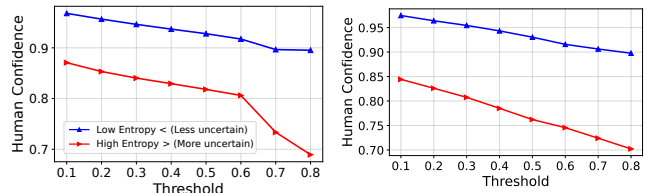
Accuracy. The primary outcomes for Yes/No and Number answer queries are detailed in Table 4, respectively. We chose these question types to ensure a fair comparison and avoid semantic mismatches in open-ended answers in Others. A distinctive feature of Bella is its reduced uncertainty estimates for correct predictions, coupled with increased uncertainty estimates for incorrect ones. Moreover, it surpasses the Single base model regarding Accuracy and Exact Match metrics.

Notably, our method is efficient, particularly in contrast to the resource-intensive baseline Bayesian models tailored for this task, *e.g.* Abbasnejad et al. (2019, 2020b,a). The computational requirements for using these baselines render the application of full SVG D or ensemble alternatives impractical, thereby highlighting the impact on practical applications by harnessing the effectiveness of Bella.

Model Uncertainty and Human Confidence. Further, we investigate the relationship between model uncertainty attained from Bella and human confidence, facilitated by multiple annotators in the VQA dataset. For this, we measure the correlation between the model disagreement by measuring the predictive entropy vs the human annotations of the answers.

VQA: Evaluation of Yes/No Questions				
Models	Ent. Corrects (↓)	Ent. Incorrect (↑)	Accuracy (↑)	Match (↑)
Single base	0.3336	0.5920	91.59	86.74
Ensemble Bella	0.3438	0.5935	91.20	86.21
SVG D Bella	0.3245	0.5950	92.46	87.83
VQA: Evaluation of Number Questions				
Single base	0.4148	0.9911	58.69	49.26
Ensemble Bella	0.4248	0.9929	57.86	48.68
SVG D Bella	0.4059	0.9816	60.19	50.99

Table 4: LLaVA-VQA Results: evaluating the accuracy and entropy of correct vs incorrect predictions.



(a) Yes/No questions.

(b) Number questions.

Figure 6: Correlation between model certainty and human confidence. This negative correlation suggests that the model’s entropy can serve as a reliable gauge of certainty, mirroring human judgment in its response to varying levels of uncertainty.

In Figure 6 we shows the correlation between the entropy of the model outputs and human confidence levels. By setting a specific threshold for the model’s entropy, we effectively bifurcate our predictions into two distinct categories: those with lower entropy fall into the ‘Low Entropy’ group, signalling reduced uncertainty within the model’s assessments, while predictions surpassing this entropy threshold are allocated to the ‘High Entropy’ segment, indicative of greater uncertainty. Intriguingly, our observations reveal a consistent negative correlation between the model’s entropy levels and human confidence across different types of queries, such as Yes/No and Number questions. This pattern suggests that the model’s entropy can serve as a reliable gauge of certainty, mirroring human judgment in its response to varying levels of uncertainty.

6 Conclusion

In this paper, we introduce an innovative approach for creating an efficient Bayesian Neural Network (BNN) approximation using only a base pre-trained model. Our approach, called Bella, demonstrates remarkable compatibility with full-rank BNN approximations like SVG D or Ensemble methods, outperforming single-network solutions across a range of tasks, from pure classification to out-of-distribution (OOD) generalization and uncertainty quantification. Our research paves the way for effective and efficient BNNs, facilitating the development of reliable and robust machine-learning models. Bella reinforces the effectiveness of employing such a simple, efficient and effective training method with diverse representations over the conventional practice of single fine-tuning.

References

- Abbasnejad, E.; Abbasnejad, I.; Wu, Q.; Shi, J.; and Hengel, A. v. d. 2020a. Gold seeker: Information gain from policy distributions for goal-oriented vision-and-language reasoning. In *Proceedings of the IEEE/CVF Conference on Computer Vision and Pattern Recognition (CVPR)*.
- Abbasnejad, M. E.; Shi, J.; van den Hengel, A.; and Liu, L. 2020b. GADE: A Generative Adversarial Approach to Density Estimation and its Applications. *Int. J. Comput. Vis.*, 128(10): 2731–2743.
- Abbasnejad, M. E.; Shi, Q.; van den Hengel, A.; and Liu, L. 2019. A Generative Adversarial Density Estimator. In *IEEE Conference on Computer Vision and Pattern Recognition, CVPR 2019, Long Beach, CA, USA, June 16-20, 2019*, 10782–10791. Computer Vision Foundation / IEEE.
- Ainsworth, S.; Hayase, J.; and Srinivasa, S. 2023. Git Re-Basin: Merging Models modulo Permutation Symmetries. In *The Eleventh International Conference on Learning Representations*.
- Antol, S.; Agrawal, A.; Lu, J.; Mitchell, M.; Batra, D.; Zitnick, C. L.; and Parikh, D. 2015. VQA: Visual Question Answering. In *International Conference on Computer Vision (ICCV)*.
- Bandi, P.; Geessink, O.; Manson, Q.; Van Dijk, M.; Balkenhol, M.; Hermesen, M.; Bejnordi, B. E.; Lee, B.; Paeng, K.; Zhong, A.; et al. 2018. From detection of individual metastases to classification of lymph node status at the patient level: the CAMELYON17 challenge. *IEEE Transactions on Medical Imaging*.
- Bishop, C. M. 2006. *Pattern Recognition and Machine Learning*. Springer.
- Blei, D. M.; Kucukelbir, A.; and McAuliffe, J. D. 2017. Variational inference: A review for statisticians. *Journal of the American statistical Association*.
- Blundell, C.; Cornebise, J.; Kavukcuoglu, K.; and Wierstra, D. 2015. Weight uncertainty in neural network. In *International Conference on Machine Learning (ICML)*.
- Challenge, G. 2024. Camelyon17 Leaderboard. <https://camelyon17.grand-challenge.org/evaluation/challenge/leaderboard/>. Accessed: 08-Mar-2024.
- Chen, P.; and Ghattas, O. 2020. Projected Stein variational gradient descent. *Advances in Neural Information Processing Systems*.
- Coates, A.; Ng, A.; and Lee, H. 2011. An Analysis of Single Layer Networks in Unsupervised Feature Learning. In *International Conference on Artificial Intelligence and Statistics (AISTATS)*.
- Daxberger, E.; Kristiadi, A.; Immer, A.; Eschenhagen, R.; Bauer, M.; and Hennig, P. 2021. Laplace Redux—Effortless Bayesian Deep Learning. In *NeurIPS*.
- Dettmers, T.; Pagnoni, A.; Holtzman, A.; and Zettlemoyer, L. 2023. Qlora: Efficient finetuning of quantized llms. *arXiv preprint arXiv:2305.14314*.
- Ding, N.; Qin, Y.; Yang, G.; Wei, F.; Yang, Z.; Su, Y.; Hu, S.; Chen, Y.; Chan, C.-M.; Chen, W.; Yi, J.; Zhao, W.; Wang, X.; Liu, Z.; Zheng, H.-T.; Chen, J.; Liu, Y.; Tang, J.; Li, J.; and Sun, M. 2023. Parameter-efficient fine-tuning of large-scale pre-trained language models. *Nature Machine Intelligence*.
- Ding, N.; Qin, Y.; Yang, G.; Wei, F.; Yang, Z.; Su, Y.; Hu, S.; Chen, Y.; Chan, C.-M.; Chen, W.; et al. 2022. Delta tuning: A comprehensive study of parameter efficient methods for pre-trained language models. *arXiv preprint arXiv:2203.06904*.
- Doan, B. G.; Abbasnejad, E. M.; Shi, J. Q.; and Ranasinghe, D. C. 2022. Bayesian Learning with Information Gain Provably Bounds Risk for a Robust Adversarial Defense. In *International Conference on Machine Learning (ICML)*.
- Fan, X.; Zhang, S.; Chen, B.; and Zhou, M. 2020. Bayesian attention modules. In *Advances in Neural Information Processing Systems (NeurIPS)*.
- Gal, Y.; et al. 2016. Uncertainty in deep learning.
- Gontijo-Lopes, R.; Dauphin, Y.; and Cubuk, E. D. 2021. No one representation to rule them all: Overlapping features of training methods. *arXiv preprint arXiv:2110.12899*.
- Goyal, Y.; Khot, T.; Summers-Stay, D.; Batra, D.; and Parikh, D. 2017. Making the V in VQA Matter: Elevating the Role of Image Understanding in Visual Question Answering. In *Conference on Computer Vision and Pattern Recognition (CVPR)*.
- Gueta, A.; Venezian, E.; Raffel, C.; Slonim, N.; Katz, Y.; and Choshen, L. 2023. Knowledge is a Region in Weight Space for Fine-tuned Language Models. *arXiv preprint arXiv:2302.04863*.
- Hendrycks, D.; and Dietterich, T. 2019. Benchmarking neural network robustness to common corruptions and perturbations. *arXiv preprint arXiv:1903.12261*.
- Houlsby, N.; Giurgiu, A.; Jastrzebski, S.; Morrone, B.; de Laroussilhe, Q.; Gesmundo, A.; Attariyan, M.; and Gelly, S. 2019. Parameter-Efficient Transfer Learning for NLP. *arXiv:1902.00751*.
- Hu, E. J.; yelong shen; Wallis, P.; Allen-Zhu, Z.; Li, Y.; Wang, S.; Wang, L.; and Chen, W. 2022. LoRA: Low-Rank Adaptation of Large Language Models. In *International Conference on Learning Representations (ICLR)*.
- Iharc0, G.; Wortsman, M.; Wightman, R.; Gordon, C.; Carlini, N.; Taori, R.; Dave, A.; Shankar, V.; Namkoong, H.; Miller, J.; Hajishirzi, H.; Farhadi, A.; and Schmidt, L. 2021. OpenCLIP.
- Izmailov, P.; Maddox, W. J.; Kirichenko, P.; Garipov, T.; Vetrov, D.; and Wilson, A. G. 2020. Subspace inference for Bayesian deep learning. In *Uncertainty in Artificial Intelligence*.
- Izmailov, P.; Vikram, S.; Hoffman, M. D.; and Wilson, A. G. 2021. What Are Bayesian Neural Network Posteriors Really Like? In *International Conference on Machine Learning (ICML)*.
- Kim, M.; and Hospedales, T. 2023. BayesDLL: Bayesian Deep Learning Library. *arXiv preprint arXiv:2309.12928*.
- Koh, P. W.; Sagawa, S.; Marklund, H.; Xie, S. M.; Zhang, M.; Balsubramani, A.; Hu, W.; Yasunaga, M.; Phillips, R. L.; Gao, I.; Lee, T.; David, E.; Stavness, I.; Guo, W.; Earnshaw, B. A.; Haque, I. S.; Beery, S.; Leskovec, J.; Kundaje, A.; Pierson, E.; Levine, S.; Finn, C.; and Liang, P. 2021. WILDS:

- A Benchmark of in-the-Wild Distribution Shifts. In *International Conference on Machine Learning (ICML)*.
- Krizhevsky, A.; Hinton, G.; et al. 2009. Learning multiple layers of features from tiny images.
- Lakshminarayanan, B.; Pritzel, A.; and Blundell, C. 2017. Simple and scalable predictive uncertainty estimation using deep ensembles. In *Advances in neural information processing systems (NeurIPS)*.
- Lin, Z.; Madotto, A.; and Fung, P. 2020. Exploring Versatile Generative Language Model Via Parameter-Efficient Transfer Learning. In *Findings of the Association for Computational Linguistics (EMNLP)*.
- Liu, H.; Li, C.; Li, Y.; and Lee, Y. J. 2023a. Improved Baselines with Visual Instruction Tuning. *arXiv preprint arXiv:2310.03744*.
- Liu, H.; Li, C.; Wu, Q.; and Lee, Y. J. 2023b. Visual Instruction Tuning. In *Advanced in Neural Information Processing Systems (NeurIPS)*.
- Liu, Q.; and Wang, D. 2016. Stein variational gradient descent: A general purpose bayesian inference algorithm. *Advances in Neural Information Processing Systems (NeurIPS)*.
- Liu, X.; Li, Y.; Chongruo, W.; and Cho-Jui, H. 2019. ADV-BNN: Improved Adversarial Defense Through Robust Bayesian Neural Network. In *International Conference on Learning Representations (ICLR)*.
- MacKay, D. 1991. Bayesian Model Comparison and Backprop Nets. In *Advances in Neural Information Processing Systems (NeurIPS)*.
- Matena, M. S.; and Raffel, C. A. 2022. Merging models with fisher-weighted averaging. *Advances in Neural Information Processing Systems (NeurIPS)*.
- Miller, J. P.; Taori, R.; Raghuathan, A.; Sagawa, S.; Koh, P. W.; Shankar, V.; Liang, P.; Carmon, Y.; and Schmidt, L. 2021. Accuracy on the line: on the strong correlation between out-of-distribution and in-distribution generalization. In *International conference on machine learning*.
- Neal, R. M. 2012. *Bayesian learning for neural networks*, volume 118. Springer Science & Business Media.
- Neal, R. M.; et al. 2011. MCMC using Hamiltonian dynamics. *Handbook of markov chain monte carlo*, 2(11).
- Papernot, N.; Faghri, F.; Carlini, N.; Goodfellow, I.; Feinman, R.; Kurakin, A.; Xie, C.; Sharma, Y.; Brown, T.; Roy, A.; Matyascko, A.; Behzadan, V.; Hambardzumyan, K.; Zhang, Z.; Juang, Y.-L.; Li, Z.; Sheatsley, R.; Garg, A.; Uesato, J.; Gierke, W.; Dong, Y.; Berthelot, D.; Hendricks, P.; Rauber, J.; and Long, R. 2018. Technical Report on the CleverHans v2.1.0 Adversarial Examples Library. *arXiv preprint arXiv:1610.00768*.
- Peng, X.; Bai, Q.; Xia, X.; Huang, Z.; Saenko, K.; and Wang, B. 2019. Moment matching for multi-source domain adaptation. In *Proceedings of the IEEE/CVF international conference on computer vision (CVPR)*.
- Radford, A.; Kim, J. W.; Hallacy, C.; Ramesh, A.; Goh, G.; Agarwal, S.; Sastry, G.; Askell, A.; Mishkin, P.; Clark, J.; Krueger, G.; and Sutskever, I. 2021. Learning Transferable Visual Models From Natural Language Supervision. In *International Conference on Machine Learning (ICML)*.
- Rame, A.; Kirchmeyer, M.; Rahier, T.; Rakotomamonjy, A.; Gallinari, P.; and Cord, M. 2022. Diverse weight averaging for out-of-distribution generalization. *Advances in Neural Information Processing Systems (NeurIPS)*.
- Rebuffi, S.-A.; Bilen, H.; and Vedaldi, A. 2017. Learning multiple visual domains with residual adapters. *arXiv:1705.08045*.
- Russakovsky, O.; Deng, J.; Su, H.; Krause, J.; Satheesh, S.; Ma, S.; Huang, Z.; Karpathy, A.; Khosla, A.; Bernstein, M.; et al. 2015. Imagenet large scale visual recognition challenge. *International journal of computer vision*.
- Seligmann, F.; Becker, P.; Volpp, M.; and Neumann, G. 2024. Beyond deep ensembles: A large-scale evaluation of bayesian deep learning under distribution shift. *Advances in Neural Information Processing Systems*, 36.
- Wang, X.; Aitchison, L.; and Rudolph, M. 2024. LoRA ensembles for large language model fine-tuning.
- Welling, M.; and Teh, Y. W. 2011. Bayesian learning via stochastic gradient Langevin dynamics. In *Proceedings of the 28th international conference on machine learning (ICML-11)*, 681–688. Citeseer.
- Wild, V. D.; Ghalebikesabi, S.; Sejdinovic, D.; and Knoblauch, J. 2023. A Rigorous Link between Deep Ensembles and (Variational) Bayesian Methods. In *Advances in Neural Information Processing Systems (NeurIPS)*.
- Wilson, A. G.; Izmailov, P.; Hoffman, M. D.; Gal, Y.; Li, Y.; Pradier, M. F.; Vikram, S.; Foong, A.; Lotfi, S.; and Farquhar, S. 2022. Evaluating approximate inference in Bayesian deep learning. In *NeurIPS 2021 Competitions and Demonstrations Track*, 113–124. PMLR.
- Wortsman, M.; Ilharco, G.; Gadre, S. Y.; Roelofs, R.; Gontijo-Lopes, R.; Morcos, A. S.; Namkoong, H.; Farhadi, A.; Carmon, Y.; Kornblith, S.; et al. 2022a. Model soups: averaging weights of multiple fine-tuned models improves accuracy without increasing inference time. In *International Conference on Machine Learning (ICML)*.
- Wortsman, M.; Ilharco, G.; Kim, J. W.; Li, M.; Kornblith, S.; Roelofs, R.; Lopes, R. G.; Hajishirzi, H.; Farhadi, A.; Namkoong, H.; et al. 2022b. Robust fine-tuning of zero-shot models. In *Proceedings of the IEEE/CVF Conference on Computer Vision and Pattern Recognition*, 7959–7971.
- Yang, A. X.; Robeyns, M.; Wang, X.; and Aitchison, L. 2024. Bayesian low-rank adaptation for large language models. In *International Conference on Learning Representations (ICLR)*.
- Ye, N.; and Zhu, Z. 2018. Bayesian adversarial learning. In *Advances in Neural Information Processing Systems (NeurIPS)*.
- Zhang, S.; Fan, X.; Chen, B.; and Zhou, M. 2021. Bayesian attention belief networks. In *International Conference on Machine Learning (ICML)*.

Bayesian Low-Rank LeArning (Bella): A Practical Approach to Bayesian Neural Networks

Overview of Materials in the Appendices

We provide a brief overview of the extensive set of additional experimental results and findings in the Appendices that follows.

1. Comparing diversity measures between SVGD Bella and its SVGD base model (Appendix A)
2. The generalization of CIFAR-10 pre-trained models on OOD dataset (STL-10) (Appendix B)
3. Uncertainty measures on the corrupted CIFAR-10-C dataset between SVGD Bella models and SVGD models (Appendix C)
4. Generalization Performance of Models on CIFAR-10-C Task (Appendix D)
5. Additional comparison studies. Including **SoTA results on (Camelyon leaderboard 2024)** (Appendix E)
6. Impact of γ parameter values on robustness of models (Appendix F)
7. Detailed information regarding RBF kernel computation in SVGD (Appendix G)
8. Detailed information about VQA task (Appendix H)
9. Detailed information regarding datasets and hyper-parameters utilized in the paper (Appendix I)

A Diversity Measures

This section assesses the diversity of the trained Bella, comparing it to the foundational SVGD model. The goal is to determine if Bella can maintain the diversity level of the SVGD base model while utilizing significantly fewer parameters.

Given the lack of a conventional metric for evaluating the diversity among parameter particles, we suggest employing the Kullback–Leibler (KL) Divergence. This measure compares the expected parameters of a Bayesian model to the softmax output for each parameter particle, serving as an indicator of model diversity. We calculate this divergence across 10,000 test samples from the CIFAR-10 dataset. In particular,

$$\text{Diversity} = \frac{1}{N} \sum_{i=1}^N KL \left[\mathbb{E}_{\theta} [p(y | \mathbf{x}_i, \theta)], p(y | \mathbf{x}_i, \theta) \right]$$

where KL is the Kullback–Leibler divergence, N is the number of samples.

Results. Figure 7 presents intriguing findings, where the SVGD Bella exhibits comparable and even greater diversity compared to the base SVGD model. We speculate that this increased diversity may stem from the Bella’s use of significantly fewer trainable parameters, reducing the likelihood of overfitting and facilitating the identification of parameter particles with enhanced diversity, all while preserving model

performance. These results further underscore the efficiency and effectiveness of our method in implementing a Bayesian neural network with substantial diversity.

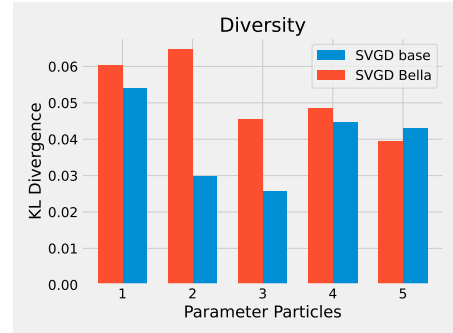


Figure 7: Diversity comparison between SVGD base and SVGD Bella. SVGD Bella show comparable and slightly better diversity measure compared to its SVGD base model.

B Generalization of CIFAR-10 Models on OOD dataset (STL-10)

In this section, we evaluate the generalization of networks trained on CIFAR-10 on a *similar* datasets, STL-10, as in (Miller et al. 2021).

STL-10 dataset. The STL-10 dataset is a benchmark for image recognition algorithms, containing 5,000 labeled training images, 8,000 labeled test images across 10 classes, and 100,000 unlabeled images for unsupervised learning. Images are 96x96 pixels, larger than those in similar datasets like CIFAR-10, facilitating more detailed models and promoting unsupervised learning techniques.

Experimental Setup. We choose eight labels in STL-10 test set, same labels observed in CIFAR-10 dataset to set a OOD dataset. This includes 6,400 images acting as the OOD dataset for CIFAR-10 pre-trained models.

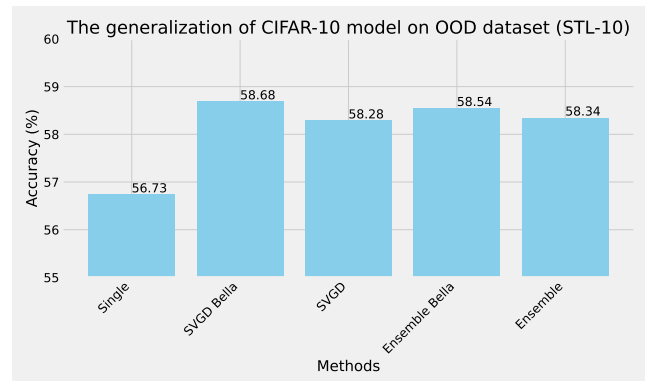


Figure 8: Enhanced OOD detection: Bella models show better performance than their counterparts on STL-10 dataset with shared CIFAR-10 labels.

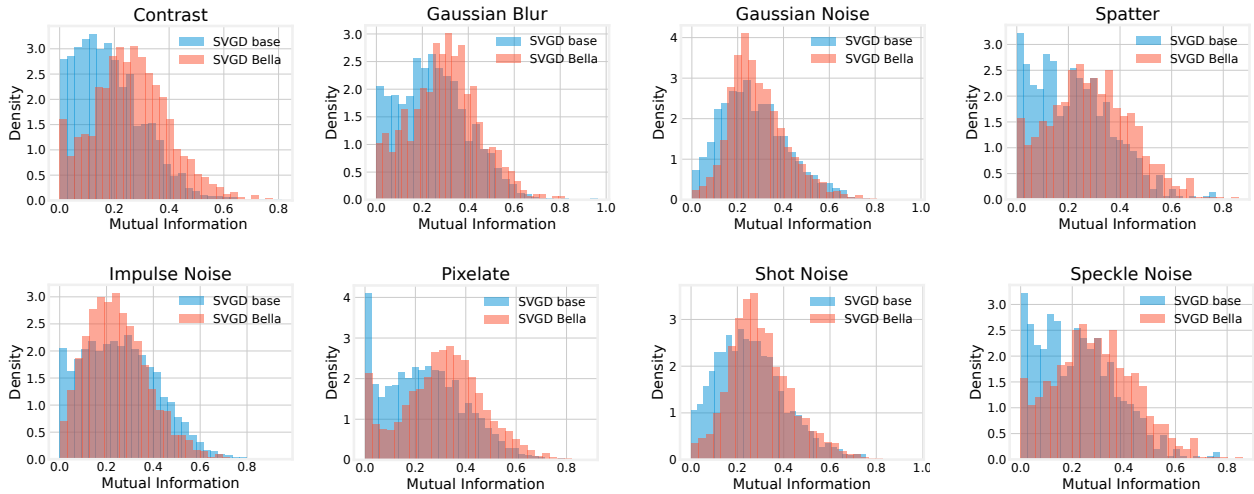


Figure 9: Out-of-distribution performance of our Bella method on the CIFAR-10-C benchmark compared with baseline SVGD models.

Models	CIFAR-10-C								Average
	Contrast	Gaussian Blur	Gaussian Noise	Impulse Noise	Pixelate	Shot Noise	Spatter	Speckle Noise	
Single base	91.78	90.58	62.96	66.48	77.94	71.56	92.14	73.87	78.53
VBL	83.77	89.34	51.10	52.08	76.43	60.94	89.21	63.19	70.76
Ensemble Bella	93.30	93.30	64.28	74.36	85.86	75.73	94.83	75.24	82.24
Ensemble base	92.69	91.92	72.90	79.08	86.49	78.83	93.45	80.49	84.61
SVGD Bella	94.69	94.05	67.89	75.86	88.70	76.49	94.85	77.61	83.77
SVGD base	97.16	93.02	75.65	81.49	86.75	81.56	95.19	82.89	86.84

Table 5: Out-of-distribution performance (in terms of accuracy) of our method Bella on the CIFAR-10-C benchmark. (Recall Bayesian approximation are from $n = 5$ particles for Ensemble and SVGD).

Results. The data presented in Figure 8 indicate that our approach slightly outperforms the SVGD and Ensemble baseline models, and significantly surpasses the capabilities of a singular network. We propose that the incorporation of a low-rank adaptation mechanism contributes to reducing overfitting, thereby enhancing the model’s generalization ability on out-of-distribution (OOD) datasets. This underscores the efficacy of our method in fostering robust generalization across OOD datasets.

C Measure Uncertainty on Corrupted CIFAR-10-C Dataset

In this section, we apply Mutual Information (MI) as a metric for assessing uncertainty. This approach enables us to compare the performance of our Bella method with models based on Stein Variational Gradient Descent (SVGD) in handling Out-of-Distribution (OOD) tasks, focusing on the CIFAR-10-C dataset. We adhere to the corruption types listed in Table 5 for this analysis.

Results. The outcomes, depicted in Figure 9, affirm the efficacy of Bella. It demonstrates comparable, and in some instances, superior performance to SVGD-based models, especially notable in most cases such as involving contrast adjustments, Gaussian blur, and pixelation. This indicates a

robust ability to detect increased uncertainty in OOD datasets, which is a valuable attribute for enhancing the reliability of machine learning models in unpredictable environments.

D Generalization Performance of Models on CIFAR-10-C Task

The generalization performance of different models in terms of accuracy across various noise types (with a maximum severity level of 5) is depicted in Table 5. The results show that Bella SVGD performs comparably to its base counterpart.

E Additional Comparison Studies

In this section, we conduct further studies on the benefits of our approach utilizing recently developed *weight averaging* concept.

Recent research has increasingly explored the concept of weight averaging, a technique where parameters from multiple models are combined to create a unified model that may offer superior predictive performance (Matena and Raffel 2022; Wortsman et al. 2022a,b). This approach is grounded in the theory that models starting from the same pre-trained state tend to have a linear loss landscape, making averaging a viable strategy. For a detailed mathematical discussion,

Model Name	CIFAR-10			CIFAR-100		
	Accuracy \uparrow	PE Correct \downarrow	PE Incorrect \uparrow	Accuracy \uparrow	PE Correct \downarrow	PE Incorrect \uparrow
Ensemble Bella soup	95.74	0.0597	0.6063	80.82	0.3461	1.2261
Ensemble base soup	97.42	0.0986	0.6917	86.42	0.3025	1.1148
SVGD Bella soup	96.32	0.0771	0.6988	83.59	0.2935	1.1044
SVGD base soup	97.62	0.0438	0.5528	86.73	0.2609	1.0426
Ensemble base	97.54	0.1125	0.5947	86.89	0.3738	1.0677
Ensemble Bella	97.58	0.0685	0.5098	86.50	0.4100	1.1218
SVGD base	97.87	0.0572	0.4692	87.32	0.3256	1.0015
SVGD Bella	97.95	0.0603	0.5193	88.09	0.4000	1.0915

Table 6: Model performance comparison among ‘soup’ models on CIFAR-10 and CIFAR-100 datasets. It should be noted that the mean of predictive entropies has been reported for correctly and incorrectly classified samples.

see (Rame et al. 2022). Corroborating this, Figure 10 features density plots and Table 6 that illustrate the predictive entropy for samples that are correctly and incorrectly classified by the CIFAR-10 and CIFAR-100 datasets using the ‘soup’ models. These results show that the performance of Bella models, post-averaging, is comparable to that of more computationally intensive baseline models. This suggests that Bella models, despite having fewer trainable parameters, are capable of achieving the same level of performance as their more complex counterparts.

Layer name		Trainable	Accuracy
FC	Proj.	Params	
0-11	0-11	1.85M	94.89
0-11	–	925K	95.11
–	0-11	925K	95.83
0-5	0-5	925K	92.7
6-11	6-11	925K	91.39

Table 7: Choosing different layers for fine-tuning with Bella, with $r = 4$, $n = 5$ on CAMELYON17 achieves *state-of-the-art performance* (Camelyon leaderboard 2024) (see highlighted row).

Ablations on fine-tuned layers. In our paper, we propose the concept of substituting the network’s complete weight matrices with low-rank adapters to approximate BNNs. This section is dedicated to assessing the effectiveness of these low-rank adapters across various layer configurations within CLIP, utilizing CAMELYON17. It should be noted that CLIP consists of 12 *ResidualAttentionBlocks*, each comprising Fully Connected (FC) and Projection (Proj.) linear layers, which we aim to modify for our Bella. The data, presented in Table 7, *reveals an interesting performance outcome from our Bella as it surpasses the SOTA in one of the experiments*. This highlights the adaptability of our proposed approach, which does not necessitate extensive fine-tuning to select specific layers for optimal performance.

Comparison of SVGD Bella and VBL. In this section, we compare the performance of SVGD Bella and VBL in distinguishing between correctly and misclassified samples. Specifically, we assess their ability to assign high entropy to mis-

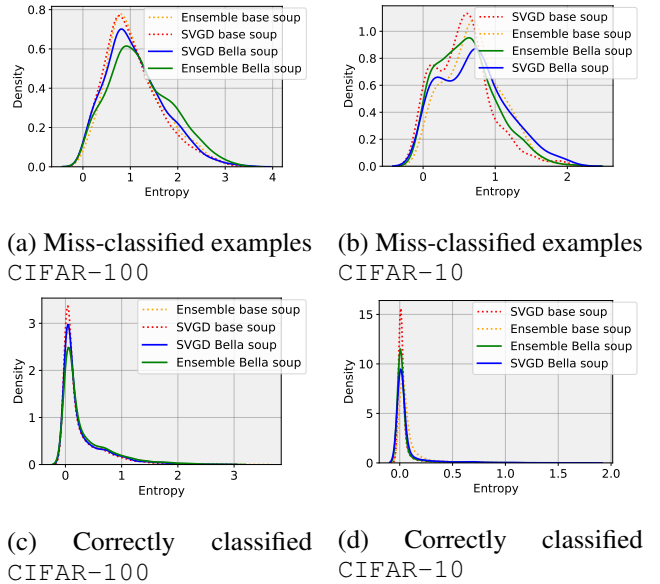


Figure 10: The density plots for predictive entropy of soup models for misclassified and density plots for correctly classified images of CIFAR-10 and CIFAR-100 show comparable performance of Bella with baselines, despite being trained with much fewer parameters.

classified samples and low entropy to correctly classified ones. Figure 11 shows that SVGD Bella outperforms VBL in this regard.

F Impact of γ Values on Robustness.

This section assesses how the repulsive force parameter, denoted as γ , influences model robustness. Experiments were carried out on the CIFAR-10 dataset using SVGD Bella with a configuration of $r = 16$, $n = 5$, while varying γ values. As illustrated in Table 8, adjustments in the repulsive force significantly affect robustness. Increasing γ enhances robustness by promoting greater diversity among parameter particles. However, prioritizing diversity to an excessive degree (i.e., γ values above 0.05) does not further enhance robustness and may even counteract improvements, although performance remains superior to scenarios with minimal repulsive force ($\gamma = 0.01$).

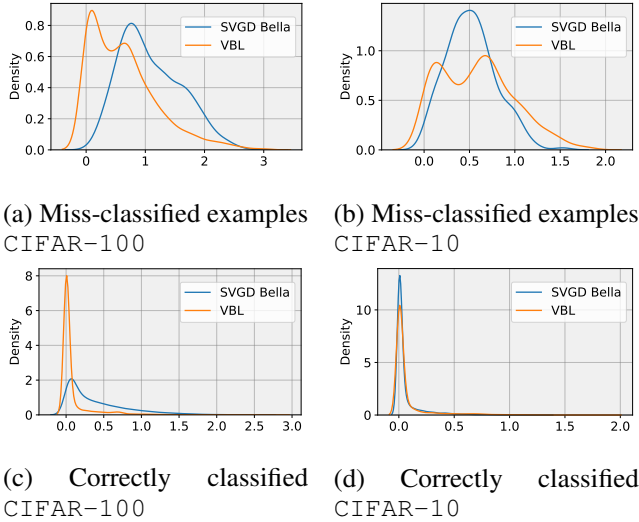


Figure 11: The density plots for predictive entropy of SVGD Bella and VBL for both misclassified and correctly classified images on CIFAR-10 and CIFAR-100 demonstrate that Bella performs on par or even better than VBL.

Pushing Parameter	Attack Budgets			
	0.001	0.005	0.01	0.03
$\gamma = 0.01$	53.7	50.4	48.1	40.9
$\gamma = 0.025$	54.9	51.3	49.2	41.8
$\gamma = 0.05$	56.1	53.7	51.2	42.5
$\gamma = 0.1$	54.4	51.9	48.1	42
$\gamma = 0.2$	55.0	50.6	47.3	40.7
$\gamma = 0.3$	54.2	52.6	49.6	42.5

Table 8: Robustness of different SVGD Bella trained on different pushing parameters (γ).

G RBF kernel computation in SVGD

We wish to evaluate RBF kernel $k(\mathbf{B}_i \mathbf{A}_i, \mathbf{B}_j \mathbf{A}_j)$ where $\mathbf{B}_i \in \mathbb{R}^{d_1 \times r}$, $\mathbf{A}_i \in \mathbb{R}^{r \times d_2}$:

$$\begin{aligned}
 k(\mathbf{B}_i \mathbf{A}_i, \mathbf{B}_j \mathbf{A}_j) &= \exp\left(-\frac{1}{2\sigma^2} \|\mathbf{B}_i \mathbf{A}_i - \mathbf{B}_j \mathbf{A}_j\|_F^2\right) \\
 &= \exp\left(-\frac{1}{2\sigma^2} \text{Tr}[(\mathbf{B}_i \mathbf{A}_i - \mathbf{B}_j \mathbf{A}_j)^\top (\mathbf{B}_i \mathbf{A}_i - \mathbf{B}_j \mathbf{A}_j)]\right).
 \end{aligned}$$

The trace term can be written as

$$\begin{aligned}
 &\text{Tr}[\mathbf{A}_i \mathbf{A}_i^\top \mathbf{B}_i^\top \mathbf{B}_i] + \text{Tr}[\mathbf{A}_i \mathbf{A}_i^\top \mathbf{B}_i^\top \mathbf{B}_j] \\
 &\quad - \text{Tr}[\mathbf{A}_j \mathbf{A}_j^\top \mathbf{B}_i^\top \mathbf{B}_j] - \text{Tr}[\mathbf{A}_i \mathbf{A}_j^\top \mathbf{B}_j^\top \mathbf{B}_i].
 \end{aligned}$$

To compute $\mathbf{A}_j \mathbf{A}_i^\top$ and $\mathbf{B}_j^\top \mathbf{B}_i$ the cost is $O(r^2 d_2)$ and $O(r^2 d_1)$ respectively. And each trace term is of the form $\text{Tr}(\mathbf{U}^\top \mathbf{V}) = \langle \mathbf{U}, \mathbf{V} \rangle_F = \text{vec}(\mathbf{U})^\top \text{vec}(\mathbf{V})$ which is an $O(r^2)$ operation and requires no further matrix multiplication.

H Detailed Information on the VQA Task

In this section, we provide more details about the experiments we conducted on the VQA task in Section 5.7.

H.1 Task Definition and Experiment Setup

Task. Visual Question Answering (VQA) (Antol et al. 2015) is a free-form and open-ended task, taking as input an image and a natural-language question about the image and producing a natural-language answer as the output. Questions in VQA require various intelligence capabilities to answer, including image recognition and object detection, as well as reasoning like commonsense reasoning. Below is an overview of the VQA dataset utilized in our paper:

- **VQA v2** (Goyal et al. 2017): This dataset contains 204,721 images, more than 1 Billion (1B) questions, and 10B ground truth answers in total. There are three main types of answers: Yes/No, Number, and Other. The evaluation set contains 80,541, 28,134 and 105,679 questions for Yes/No, Number, and Other respectively.

As open-ended questions may result in a diverse set of possible answers, VQA gather 10 human annotations for each question as the ground-truth answers. These answers can be different from each other, and even incorrect.

Models. In our experiments, we applied Bella on top of LLaVA (Liu et al. 2023b,a) to address the VQA task. Specifically, we utilized the LLaVA-1.5 7B model, an improved version of the original LLaVA with superficial modifications. We followed the public training method using a deepspeed codebase.

However, manipulating parameter gradients is non-trivial, and there is no public way of doing this using deepspeed. Therefore, we simulated the low-rank approximation from the same initialization by conducting several end-to-end fine-tuning settings with different random seeds, learning rates, and gradient accumulation steps. Together with the official public model, based on our Bella, there are four generated variants we call Bella-0, Bella-1, Bella-2, Bella-3 respectively.

Metrics. Below are a detailed metrics used during our evaluations.

- **Accuracy:** In VQA dataset, there are 10 human annotations for each question. The model prediction accuracy is calculated by

$$\text{Accuracy}(\text{ans}) = \min\left\{\frac{\#\text{humans that said } \text{ans}}{3}, 1\right\}. \quad (3)$$

In order to be consistent with human accuracy, this metric is averaged over all 10 chosen 9 sets of human annotations.

- **Exact Match:** We defined the metric as follows:

$$\text{EM} = \begin{cases} 1, & \text{if Accuracy} = 1. \\ 0, & \text{otherwise.} \end{cases} \quad (4)$$

When *Accuracy* equals 1, it means the predicted answer is 100%, same with the ground-truth annotation, i.e., Exact Match with one another.

To measure the model uncertainty along with the human confidence in Figure 6, we define **Entropy** and **Human Confidence** as follows.

- **Entropy:** Given a single question, we can calculate the entropy of the model prediction after applying *softmax* over the logits of LLaVA:

$$Entropy = \frac{1}{N} \sum_i^N \sum_j^V -p_{ij} \times \ln(p_{ij}) \quad (5)$$

Note that N is the output sequence length, V is the vocabulary size, and p_{ij} is the output of softmax function. We expect the entropy to be lower for correct predictions, as it stands for lower uncertainty. We expect the entropy to be higher for incorrect predictions, i.e., more uncertain on the prediction.

- **Human Confidence (HC):** We calculate the confidence of 10 human annotators as follows:

$$HC = \frac{1}{10} \max\{\#humans\ that\ said\ ans\} \quad (6)$$

More annotators agree with the same answer, higher HC will be.

H.2 Experiments

Correlation. Given a question, our model generates a prediction accompanied by logits. We calculate the *Entropy* using the logits and assess *Human Confidence* by leveraging 10 ground-truth responses for this prediction. After compiling all predictions, we introduce a specific *threshold*, segregating them into two distinct categories: those not meeting the *threshold* are classified under ‘Low Entropy’, while those exceeding it are allocated to the ‘High Entropy’ segment. In Figure 6, the *threshold* values are set within the range $\{0.1, 0.2, \dots, 0.8\}$. For each threshold level, we compute the average *Human Confidence* for both ‘Low Entropy’ and ‘High Entropy’ segments, and these averages are plotted as distinct curves.

Similarity. Initially, we computed the pairwise distances among the trained Bella models. We employed cosine similarity, which varies between 0 and 1, as our metric. As shown in Table 10, the choice of training strategies influences the degree of similarity among model parameters. Notably, Bella-0 exhibits the greatest dissimilarity when compared to the rest, whereas Bella-2 and Bella-3 display the highest similarity.

Models	Correct Entropy	Incorrect Entropy	Accuracy	Exact Match
Single base	0.5782	1.4826	70.00	57.17
Ensemble Bella	0.6079	1.5457	67.05	55.26
SVG D Bella	0.5359	1.4602	68.38	56.68

Table 9: Performance of different LLaVA models on ‘Other’ questions of VQA tasks.

H.3 Results

The performance of different single models and ensembles are presented in Table 4, Table 9. We ensembled two Bella models by simply averaging two softmax output scores. Given the model similarity matrix in Table 10, some observations and conclusions can be made from these tables.

	Bella-0	Bella-1	Bella-2	Bella-3
Bella-0	1	0.0286	0.0327	0.0317
Bella-1	0.0286	1	0.6289	0.5508
Bella-2	0.0327	0.6289	1	0.8047
Bella-3	0.0317	0.5508	0.8047	1

Table 10: Cosine Similarities between different Bella trained weights.

- Across all models, the averaged entropy of correct predictions is lower than the incorrect predictions. It shows models usually have higher certainty in correct predictions but lack confidence in wrong predictions.
- To some extent, entropy can be used as an indicator of the model’s accuracy. For example, models with high accuracy often have lower entropy for correct predictions and higher entropy for incorrect predictions.
- We find that an ensemble of two dissimilar models, e.g., SVG D Bella (Bella-0, Bella-1) (parameters are away from each other), usually ends with higher accuracy and exact match scores, as well as lower entropy over correct predictions. While two similar models ensemble ends with lower accuracy and exact match scores, e.g., Ensemble Bella (Bella-2, Bella-3).
- For other questions in VQA, the EM score of the SVG D Bella is slightly lower than the Single base. As models would generate longer textual answers for those questions, it is non-trivial to investigate a better ensemble strategy. In Figure 12, we present some incorrect predictions yet reasonable generation by SVG D Bella, where human annotators show high uncertainty as well.

In addition, we show the evaluation of uncertainty using Mutual Information in Figure 13 and provide case studies in Figure 12 and Figure 14 to show predicated answers from different models. The Figure 13 show the efficacy of Bella. It enables large-scale networks like LLaVA to predict outcomes with *uncertainty* for both VQA ‘Yes/No’ and ‘Number’ questions, a capability that a single base model lacks.





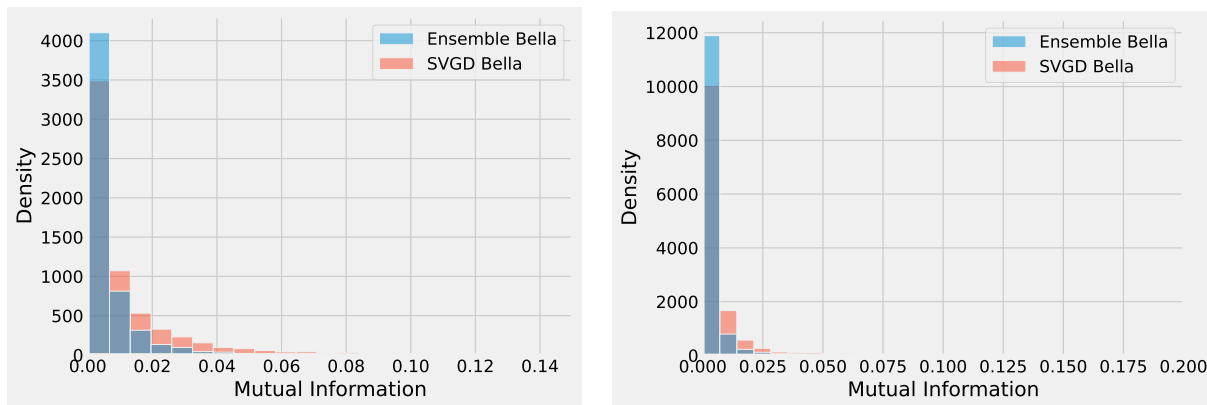
Image	Question	Ensemble Bella Answer (Entropy / MI)	SVG D Bella Answer (Entropy / MI)	Ground Truth
	What does it say below the red circle?	Electric par only while charging (0.9650 / 0.0077)	Electric vehicle parking only while charging (0.4221 / 0.0064)	Electric vehicle parking only while charging: 6/10 P: 2/10 No parking: 1/10 No electric parking: 1/10
	What kind of sign is above the doorway?	Fire (1.6809 / 0.0382)	Exit (1.2282 / 0.0388)	Exit: 9/10 Neon: 1/10
	What color is the dome shaped roof in the back?	Red (2.0491 / 0)	Brown (2.0405 / 0.0233)	Gray: 3/10 Green: 1/10 Brown: 2/10 Red : 1/10 Black: 2/10 Blue: 1/10
	What are these animals?	Giraffes (0.2438 / 0.5087)	Giraffe (0.2592 / 0.0143)	Giraffes: 9/10 Giraffe: 1/10

Figure 12: In comparing LLaVA-VQA predictions on ‘Other’ questions: SVG D Bella outperforms Ensemble Bella, even with more extended predictions. In one case, both Bella err, but with notable human annotator disagreement. Interestingly, SVG D Bella shows greater uncertainty (MI), unlike the confident Ensemble Bella (MI=0). Given that 2 out of 10 annotators chose “Brown,” SVG D Bella’s answer is deemed acceptable. In another case, SVG D Bella correctly identifies “Giraffe” albeit singularly, mirroring a minor error also seen among human annotators.



(a) Yes/No questions.





(b) Number questions.

Figure 13: Evaluation of uncertainty estimations on misclassified examples using Mutual Information on VQA tasks. Overall, the SVG D Bella outperforms the Ensemble Bella as it shows higher uncertainty (distribution shifting →).


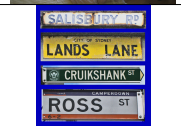


I Detailed Parameters and Datasets

In this section, we mention in detail the description for each of the dataset utilized in our experiment as below:

- **CIFAR-10:** This dataset comprises 60,000 32×32 color images divided into 10 distinct classes, with each class containing 6,000 images. It is partitioned into 50,000

Image	Question	Ensemble Bella Answer (Entropy / MI)	SVG D Bella Answer (Entropy / MI)	Ground Truth
	Is there a chain link fence in the image?	Yes (0.6440 / 0.0046)	No (0.6337 / 0.0271)	No: 10/10
	Does she eat with the right hand?	No (0.6624 / 0.0061)	Yes (0.7079 / 0.0167)	Yes: 10/10
	Is the train moving fast?	No (0.7015 / 0.0001)	Yes (0.6982 / 0.0006)	Yes: 9/10 Maybe: 1/10
	Are there any boxes in the room?	No (0.6965 / 0.0008)	Yes (0.6901 / 0.0086)	No: 10/10

(a) In assessing LLaVA-VQA predictions for ‘Yes/No’ questions, SVG D Bella tends to produce accurate responses but with a notable increase in uncertainty (reflected by higher MI values). Particularly striking is the last case study, where SVG D Bella exhibited a tenfold increase in uncertainty (MI) compared to the Ensemble Bella, when it makes an incorrect prediction.

Image	Question	Ensemble Bella Answer (Entropy / MI)	SVG D Bella Answer (Entropy / MI)	Ground Truth
	How many seats are there?	2 (0.4897 / 0.0002)	1 (0.2980 / 0.0092)	1: 10/10
	How many signs?	3 (0.6127 / 0.0023)	4 (0.5676 / 0.0063)	4: 10/10
	How many skyscrapers are there?	3 (0.6818 / 0.0152)	2 (0.6535 / 0.0513)	2: 6/10 0: 4/10
	How many boys are on the field?	3 (0.5166 / 0.0061)	4 (0.5191 / 0.0203)	3: 10/10

(b) For LLaVA-VQA predictions on ‘Number’ questions, SVG D Bella surpasses Ensemble Bella in performance. A noteworthy observation from the final case study is the elevated uncertainty associated with SVG D Bella during instances of incorrect predictions, indicating its lack of confidence in those particular responses. In the third case study, SVG D Bella exhibited high uncertainty (MI), reflecting the varying opinions among human evaluators.

Figure 14: Model predictions and uncertainty on ‘Yes/No’ and ‘Number’ questions.

training images and 10,000 test images. The classes cover a range of subjects from animals to vehicles, providing a fundamental challenge in image classification.

- **CIFAR-10-C**: This dataset is an extension of the CIFAR-10 dataset, designed to evaluate the robustness of machine learning models against common image corruptions. It contains the same 60,000 images as CIFAR-10, however, the images in CIFAR-10-C have been systematically altered using a range of corruption techniques, including noise, blur, weather, and digital effects, resulting in 19 different corruption types each at 5 severity levels. This dataset is used to test the performance of models in recognizing objects under various real-world conditions, making it a valuable tool for improving the reliability and robustness of image recognition systems.
- **STL-10**: This dataset is a benchmark for evaluating image recognition algorithms, featuring 13,000 color images. This dataset is divided into 5,000 training images and 8,000 test images, distributed across 10 different classes that include a variety of objects such as animals and vehicles. Each image in the dataset is 96×96 pixels, offering higher resolution than many similar datasets such as CIFAR-10. The STL-10 dataset is tailored for supervised learning tasks in image recognition, providing a structured framework for developing and testing algorithms' ability to classify images into predefined categories.
- **CIFAR-100**: Similar to CIFAR-10, the CIFAR-100 dataset is composed of 100 classes, each with 600 images, offering a more detailed classification challenge compared to CIFAR-10.
- **CAMELYON17**: The CAMELYON17 dataset is utilized in a domain generalization context, where the domains are represented by different hospitals. The primary objective is to develop models capable of generalizing to data from hospitals not included in the training set. Focusing on binary classification, the dataset comprises 96×96 histopathological images as input, with the task to identify the presence of tumor tissue in the central 32×32 region, indicated by a binary label.
- **ImageNet (ILSVRC2012)**: which is a subset of the ImageNet dataset specifically used for the ImageNet Large Scale Visual Recognition Challenge in 2012, contains over 1.2 million images distributed across 1,000 different classes.
- **DomainNet**: DomainNet is one of the largest and most diverse datasets available for domain adaptation studies. It contains approximately 600,000 images across 345 categories, spanning six distinct visual domains (Real, Clip-Art, Infograph, Paint, Sketch, Quick). This diversity in domains and categories enables the dataset to simulate real-world scenarios where models must adapt to different visual representations and styles.

Hyper-Parameters.

Detailed information about the hyper-parameters used can be found in Table 11.

Name	Value	Notes
r	ImageNet:16, Others:4	Rank values
γ	0.01	Weight to control the repulsive force
n	5	#Parameter particles
<i>optimizer</i>	AdamW	With adaptive scheduler

Table 11: Hyper-parameters setting in our experiments.